Cytokine 113 (2019) 74–82

Contents lists available at ScienceDirect

Cytokine

journal homepage: www.elsevier.com/locate/cytokine

The hyaluronic acid-rich node and duct system is a structure organized for innate immunity and mediates the local inflammation

Beom K. Choi[a,1], Sun H. Hwang[d,1], Yu I. Kim[c], Rohit Singh[b], Byoung S. Kwon[d,e,*]

[a] Biomedicine Production Branch, National Cancer Center Institute, Goyang 10408, Republic of Korea
[b] Immunotherapeutics Branch, Division of Convergence Technology, National Cancer Center Institute, Goyang 10408, Republic of Korea
[c] Graduate School of Cancer Science and Policy, National Cancer Center Institute, Goyang 10408, Republic of Korea
[d] Eutilex, Co., Ltd., Suite# 1401, Daeryung Technotown 17 Gasan digital 1-ro 25, Geumcheon-gu, Seoul 08594, Republic of Korea
[e] Department of Medicine, Tulane University Health Sciences Center, New Orleans, LA, USA

ARTICLE INFO

Keywords:
Hyaluronic Acid-rich Node and Duct System
Primo Vascular System
Innate immunity
TLR
Lymphoid tissue

ABSTRACT

The Hyaluronic Acid-rich Node and Duct System (HAR-NDS or NDS), Primo Vascular System (PVS) or Bonghan System (BHS), is thought to be a third circulatory system independent of the blood and lymphatic systems and a structure of connected nodes and ducts. Although it seems to be part of the immune system as it is enriched with cells of innate immunity, little is known about its immunological roles. We performed cellular profiling and secretome analysis of NDS in a steady state and under TLR2- or TLR4-mediated local inflammation, and found that the NDS is pre-dominantly enriched with the myeloid cells, selectively attracts the inflammatory macrophages and neutrophils, has a flexible structure just like the lymph node, and is structured with the fibroblastic reticular cells and reticular network. NDS dominantly harbored the myeloid cells in both steady and activated status, and secreted various types of inflammatory cytokines by proinflammatory stimuli. These results suggest that NDS is the lymphoid structure for the innate immunity and plays an intermediary role in the innate immune cell-mediated local inflammation.

1. Introduction

In 1962 Kim described novel anatomical structures corresponding to the ancient acupuncture meridians, which he named the Bonghan System (BHS) [1,2]. He suggested that the BHS was an independent functional and morphological system, interconnected through nodes and ducts, containing endothelial cells with rod-shaped nuclei, and enriched with biochemical substances such as DNA and RNA, fat, sugar and hyaluronic acids, and including Sanals (microcells) that were thought to have the characteristics of embryonic stem cells [3]. However, due to a lack of suitable methods, the existence of the BHS was not fully supported by evidence and the underlying observations were not easily reproduced by other researchers.

In 2002, Soh et al. revived the concept of the Bonghan system with new methodology, and renamed it the Primo Vascular System (PVS) [4]. They first observed the PVS in the blood vessels of rabbits and then identified it on the surface of various rabbit organs including intestines, liver, stomach, and bladder, and even in lymphatic vessels [3]. Soh and Lee [5–8] developed a number of new experimental approaches and identified several characteristics of the PVS including its presence in/on tumor tissues [9], expression of stem cell markers [10], endothelial and mesenchymal properties of the primo vessels [11], and the internal structure of the PVS [12].

More recently, Kwon et al. demonstrated that the PVS is enriched with innate immune cells and hematologic progenitors [13,14], and renamed the Hyaluronic Acid-rich Node and Duct System (HAR-NDS or NDS) because the nodes and ducts contained high levels of hyaluronic acid as visualized by alcian blue staining. Although the NDS has been considered to correspond to the ancient acupuncture meridians or to be a third circulatory system, it is highly enriched with innate immune cells and thus seems to be part of immune system. Nevertheless, the immunological roles and physiological significance of the NDS are still not defined. In this study, we analyzed the cellular composition of NDS in a steady and activated status, cytokine and chemokine production

Abbreviations: HAR-NDS/NDS, The Hyaluronic Acid-rich Node and Duct System; PVS, Primo Vascular System; BHS, Bonghan System; LPM, large peritoneal macrophage; SPM, small peritoneal macrophages; MALT, mucosa-associated lymphoid tissue; PAMP, pathogen-associated molecular pattern; PBMC, peripheral blood mononuclear cells; PEC, peritoneal exudate cell; RN, reticular network; DAMPs, damage-associated molecular patterns

* Corresponding author at: Eutilex, Co., Ltd., Suite# 1401, Daeryung Technotown 17 Gasan digital 1-ro 25, Geumcheon-gu, Seoul 08594, Republic of Korea.
E-mail address: bskwon@eutilex.com (B.S. Kwon).
[1] These two authors contributed equally to the work.

https://doi.org/10.1016/j.cyto.2018.06.011
Received 22 December 2017; Received in revised form 7 June 2018; Accepted 8 June 2018
Available online 12 June 2018

under the inflammatory condition, and physiological and cellular changes of NDS by proinflammatory stimuli *in vivo*.

2. Materials and methods

2.1. Isolation of NDS

Four-to-five-week-old male C57BL/6 mice were purchased from OrientBio (Gapyeong, Korea). TLR2$^{-/-}$, TLR4$^{-/-}$, and RAG1$^{-/-}$ mice on a C57BL/6 background were obtained from the Jackson Laboratory (Bar Harbor, ME). All animal experiments were reviewed and approved by the Animal Care and Use Committee of the National Cancer Center (NCC-15-264) and were performed in accordance with the Guide for the Care and Use of Laboratory Animals. Wild-type, TLR2$^{-/-}$, TLR4$^{-/-}$, and RAG1$^{-/-}$ mice were anesthetized by intramuscular (i.m.) injection of Zoletil (2.5 mg/kg) and Rompun (0.5 mg/kg). To collect NDS in the peritoneal cavity, an incision was made along the abdominal linea alba and the NDS was collected between the anterior wall and the intestine or liver without alcian blue staining under a stereomicroscope (Zeiss Stereo Discovery V20) with a camera (Zeiss AxioCamHRc camera), as previously reported [8].

2.2. Flow cytometry of NDS node cells

The isolated NDS nodes were placed in 0.5 ml RPMI1640 medium supplemented with 0.1% type IV collagenase (Sigma-Aldrich, St. Louis, MO) and 40 μg/ml DNase I (Takara Bio, Shiga, Japan) and the mixtures were incubated in a 37 °C incubator for 15 min. The digested NDS nodes were washed with RPMI1640 containing 10% FBS medium and used in flow cytometry. To analyze the immune subsets in the NDS nodes, the NDS cells were first incubated with 2.4G2 Fc Block for 5 min and then stained with PE-conjugated anti-CD3, anti-CD19, anti-NK1.1, anti-CD11b, anti-F4/80, anti-Ter119, or anti-Gr-1 mAb along with FITC-conjugated anti-CD90 mAb for 30 min. To compare the phenotype of macrophages in blood, peritoneal cavity and NDS, the cells were stained with anti-CD3-PE-Cy7, anti-CD19-PE-Cy7, anti-CD11b-PE-Cy5, anti-Ly-6C-FITC, anti-Ly-6G-PE, anti-F4/80-BV421, anti-MHC II-APC. All antibodies for flow cytometry were purchased from BD Biosciences except anti-CD3 (BioLegend), anti-CD19 (BioLegend), anti-MHC II (eBioscience).

2.3. Measurement of cytokines and chemokines

NDS nodes were collected from the peritoneal cavity of 4-week-old C57BL/6 as described above. Each node was placed in 1 ml of RPMI1640 supplemented 10% FBS and treated with 1 μg/ml LPS or 50 μg/ml zymosan for 6 h. Cytokines and chemokines in supernatants were detected using a Proteome Profiler Mouse Cytokine Array Kit, Panel A and Proteome Profiler™ Mouse Chemokine Array Kit (R&D Systems) according to the manufacturer's instructions. Relative densitometric value = densitometric value of reference spot/densitometric value of a sample spot.

2.4. Treatment of mice, and flow cytometry

Four-week-old male C57BL/6 mice were intraperitoneally (i.p.) injected with 25 μg of LPS (List Biological Laboratories, Inc., Campbell, CA) or 200 μg of zymosan (InvivoGen, San Diego, CA), and NDS nodes were collected from the peritoneal cavity of the mice 0, 6, 24 or 48 h later. In a separate experiment, MC38 mouse colon adenocarcinoma cells were cultured in high-glucose $DMEM_{10}$ medium, harvested, washed twice with PBS, and irradiated with 30 Gy. Wild-type, TLR2$^{-/-}$, and TLR4$^{-/-}$ C57BL/6 mice were i.p. injected with 1×10^7 irradiated apoptotic MC37 cells and NDS nodes were collected from the peritoneal cavity of the mice at day 1, 2, and 3. The NDS nodes were digested with collagenase and DNase I as described above and stained with fluorescence-conjugated anti-CD11b, anti-F4/80, and anti-Gr-1 mAbs. Samples were subsequently analyzed by FACSCalibur (BD Bioscience) and CD11b$^+$ cells were gated and plotted as F4/80 vs. Gr-1.

2.5. Confocal microscopy of HAR-Ns

NDS nodes were collected from the peritoneal cavity of C57BL/6 24 h after i.p. injection of 1×10^7 irradiated apoptotic MC38 tumor cells. Frozen sections were prepared from WT NDS node and stained with anti-F4/80, anti-CD11b, or anti-ER-TR7 mAbs, followed by rhodamine-conjugated secondary mAb. Samples were mounted with DAPI-containing solution, and images were captured with a laser scanning microscope (Zeiss LSM 780, Carl Zeiss, Germany). For whole mount and sectional views of node structure, NDS nodes were fixed in paraformaldehyde, permeabilized with 1% Triton X-100 in PBS and stained for the fibroblastic reticular cell-specific marker ER-TR7 and rhodamine-conjugated secondary mAb. Z-stack images were acquired with the laser scanning microscope and projected as maximum intensity projections.

2.6. Adoptive cell transfer

Peritoneal exudate cells (PECs) were collected from C57BL/6 mice 48 h after injection of 20 μg LPS or 200 μg zymosan, labeled with 10 μM CFSE, and i.p injected into C57BL/6 mice. After 24 h, NDS nodes were photographed under a stereo microscope, their size was calculated and flow cytometry was performed.

2.7. Statistical analysis

All data were analyzed with the statistical program, Prism 4.0 GraphPad (San Diego, CA, USA). Student's *t*-test was used to determine the statistical significance of differences between groups.

3. Results

3.1. The NDS degenerates as mice age, and lymphocyte deficiency delays degeneration

When we attempted to isolate the NDS from the peritoneal cavity of C57BL/6 mice they were readily located in 4-week-old mice but rarely in 7–8-week-old mice. Therefore, we wondered whether the NDS degenerates in ageing mice. To check this hypothesis, we examined the sizes of NDS in 4–8 week-old mice. Consistent with the previous finding, the NDS from 4 to 6 week-old mice had a typical node and duct structure, whereas at 7–8 weeks they were thread-like due to reduced node structures (Fig. 1A) and were rarely detectable in mice of > 9 weeks. Since the NDS was known to be enriched with myeloid cells such as mast cells, eosinophils, neutrophils and histiocytes [13], we wondered whether degeneration of the NDS would be delayed in lymphocyte-deficient RAG1$^{-/-}$ C57BL/6 mice. The NDS from > 4 week-old RAG1$^{-/-}$ mice turned out to be larger than those of normal mice and NDS could be observed even in 10-week-old mice (Fig. 1B). Repeated measurements of NDS node diameters indicated that the average diameter of the NDS nodes tended to be higher in RAG1$^{-/-}$ mice than in C57BL/6 mice, but the difference was only statistically significant in 8-week-old mice (Fig. 1C).

To assess the cellular composition of NDS, we performed flow cytometry with freshly-isolated NDS node cells. When the NDS was mechanically digested, there were fewer live cells than we expected. However, when they were digested with collagenase and DNase I, many live cells could be isolated. Flow cytometry indicated that there were two populations of cells in the NDS - small and large cells (Fig. 1D). The small, FSC^{Low} cells were negative for CD3, CD19, NK1.1, CD11b, and F4/80, whereas the large, FSC^{High} cells were mainly positive for CD11b or F4/80 (Fig. 1D). Since NDS degenerated in ageing mice and their

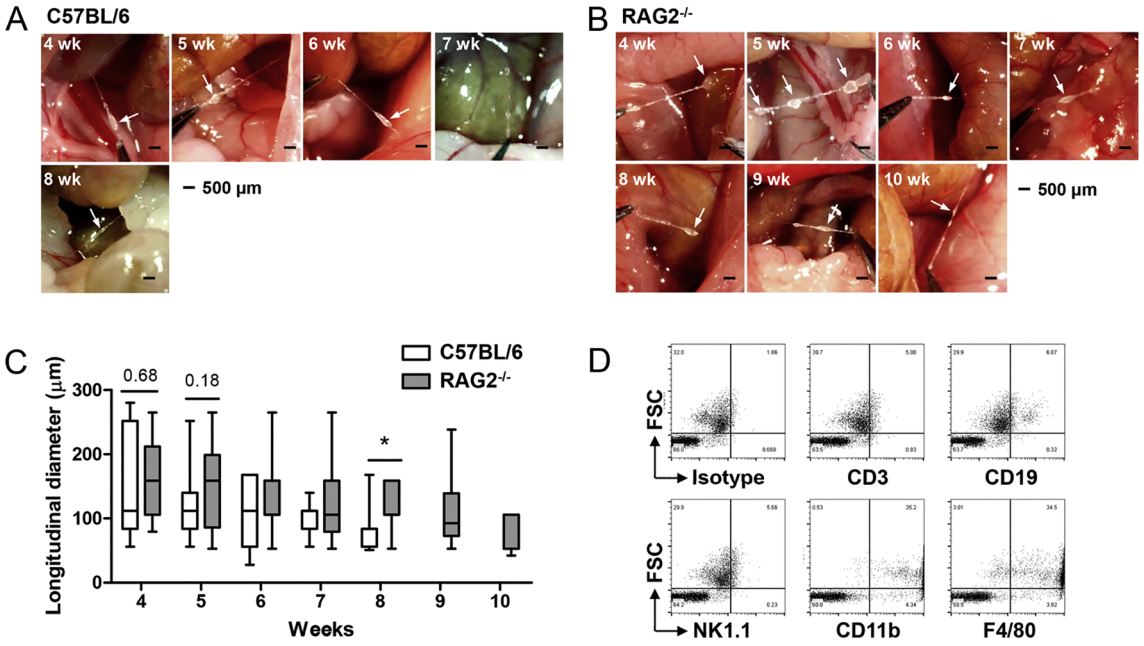

Fig. 1. Degeneration of the NDS in wild-type and RAG1$^{-/-}$ C57BL/6 mice. NDS was collected from the peritoneal cavity of 4-to-10-week-old C57BL/6 or RAG1$^{-/-}$ B6 mice and photographed using a stereomicroscope. (A and B) Representative images of the NDS collected from 4-to-10-week-old C57BL/6 (A) and RAG1$^{-/-}$ mice (B) (n = 4–8 for each week, magnification × 25). (C) The sizes of the NDS node were calculated from (A) and (B). (D) NDS nodes from 4-week-old C57BL/6 or RAG1$^{-/-}$ mice were digested with 0.1% type IV collagenase and 40 μg/ml DNase I for 15 min in RPMI1640 medium. Single cell suspensions were stained with the indicated antibodies and subsequently analyzed by FACSCalbur (BD Bioscience). Data are representative of three independent experiments. Results in (C) are means ± SDs.

major cell populations were CD11b$^+$ and F4/80$^+$, we expect that NDS may be not the local branches extended from lymphatic network.

3.2. Tissue macrophages are the major population in NDS

We examined the lymphoid and myeloid cells in NDS nodes. Flow cytometry showed that there were many cells with strong auto-fluorescence (Fig. 2A), which indicated that macrophages would reside in NDS nodes. CD90 staining suggested that T cells were rarely found (Fig. 2A). NDS nodes contained at most 1 or 2% of CD90$^+$CD3$^+$ T cells, CD19$^+$ B cells, NK1.1$^+$ NK cells, and Gr-1$^+$ granulocytes (Fig. 2A). As expected, CD11b$^+$F4/80$^+$ macrophages were the dominant population in the NDS node (Fig. 2A). It was noteworthy that TER119$^+$ RBCs were also abundant (Fig. 2A). These results suggested that CD11b$^+$F4/80^{High} macrophages and RBCs were the major populations in NDS (Fig. 2B and C).

To further characterize whether CD11b$^+$F4/80^{High} macrophages in NDS were the tissue macrophages or newly recruited monocyte-derived macrophages, peripheral blood mononuclear cells (PBMCs), peritoneal exudative cells (PECs) and NDS node cells were stained with several markers including CD3, CD19, CD11b, Ly-6C, Ly-6G, F4/80 and MHC II. Flow cytometry showed that blood monocytes were CD11b^{Low}CD3$^-$CD19-Ly-6G^{Low}Ly-6C^{High}F4/80^{Low}MHC-II^{Low} phenotype, while macrophages from PECs and NDS were identical by showing CD11b^{High}CD3$^-$CD19-Ly-6G$^-$Ly$^-$6C$^-$F4/80^{High}MHC-II$^{+/-}$ phenotype (Fig. 2D). Major population in PECs is known as the large peritoneal macrophages (LPMs) with CD11b^{High}Ly-6G^{Low}Ly-6C$^-$F4/80^{High}MHC-II^{Low} phenotype and suspects to be originated from yolk sac rather than bone marrow [15]. Consequently, these results indicate that the tissue macrophages were the major population in NDS.

3.3. NDS produces pro-inflammatory cytokines and chemokines

Since the tissue macrophages were the major cell population in NDS, we asked whether NDS would respond to proinflammatory stimuli such as LPS and zymosan. Single NDS freshly isolated from C57BL/6 mice was placed in medium and treated with zymosan (dectin-1 and TLR2 ligand) or LPS (TLR4 ligand) for 6 h, and cytokines and chemokines were measured in the supernatants. Several cytokines and chemokines were continuously expressed by NDS, or induced by zymosan or LPS treatment (Fig. 3 upper and lower panels). Expression of G-CSF, IL-1Rα, IL-6, CXCL1, CXCL2, and TNF-α was strongly increased by zymosan or LPS treatment (Supplemental Table 1), while CCL6, CXCL12, CCL9(/10), IL-16, and CCL2 were continuously expressed (Supplemental Table 2).

Most of cytokines and chemokines induced by proinflammatory stimuli are involved in the activation, migration and differentiation of myeloid cells, particularly neutrophils. G-CSF modulates the survival, proliferation and differentiation of the neutrophil lineage [16], and CXCL1 and CXCL2 promote inflammation by attracting neutrophils [17,18]. IL-6 and TNF-α together induce acute inflammation by enhancing fever, the phagocytic activity of macrophages, and attraction of neutrophils [19,20]. IL-1 receptor antagonist (IL-1Ra) appears to be produced to prevent tissue damage [21]. CCL6, CXCL12, CCL9/10, IL-16, and CCL2, which are continuously produced by NDS, appear to be primarily involved in the differentiation and migration of monocytes and macrophages [22–27]. The level of CCL6, produced constitutively by NDS, was the highest among the chemokines (Fig. 3). Although the functions of CCL6 *in vivo* are not well understood, its constitutive production and chemotactic activity for macrophages suggest that it is involved in the selective accumulation of macrophages in NDS.

Taken together, these results indicate that NDS constantly produces chemokines such as CCL6 that attract monocytes/macrophages, and that proinflammatory stimuli strongly increases the production of proinflammatory cytokines and chemokines that induce the differentiation and migration of macrophages and neutrophils.

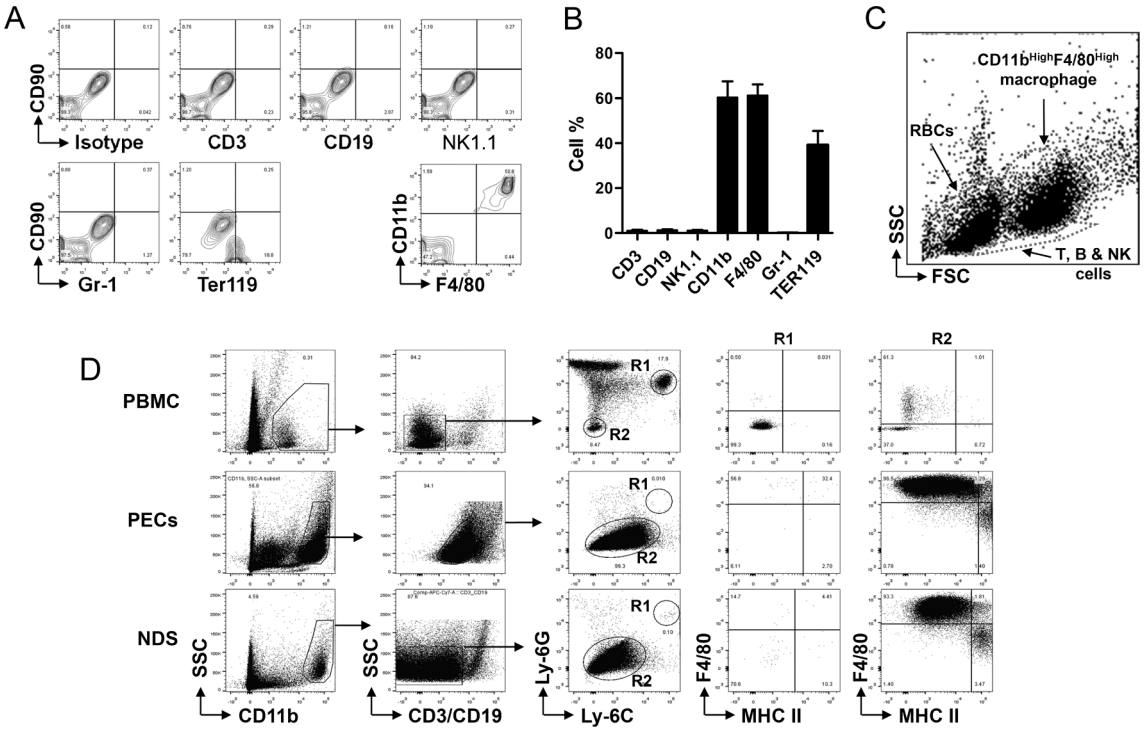

Fig. 2. Immune cell subsets in NDS node. (A) NDS nodes from 4-week-old C57BL/6 were digested with collagenase and DNase I as described above, stained with the indicated antibodies along with anti-CD90 mAb, and subsequently analyzed by FACSCalbur (BD Bioscience). (B) Percentages of immune cell subsets were calculated from (A). (C) NDS node cells were plotted FSC vs. SSC. RBCs, macrophages and lymphocytes were indicated with the arrow. (D) Phenotype of macrophages from blood, peritoneal cavity and NDS nodes were assessed by staining the cells with fluorescence-conjugated anti-CD3, CD19, CD11b, Ly6G, Ly6C, F4/80 and MHC II mAb. Data are representative of three independent experiments (n = 3). Results in (B) are means ± SDs.

3.4. Proinflammatory stimuli in vivo induces rapid and transient swelling of NDS nodes by recruiting neutrophils and macrophages

We next examined whether proinflammatory stimulation *in vivo* with LPS or zymosan induced morphological and cellular changes of NDS. Surprisingly, i.p. injection of LPS or zymosan radically altered the size and color of NDS nodes within 24 h (Fig. 4A). In the steady state, the NDS nodes were 50–100 μm in diameter and transparently white (Fig. 4A; upper panel). However, following injection of LPS or zymosan, they swelled rapidly and became a milky white (Fig. 4A).

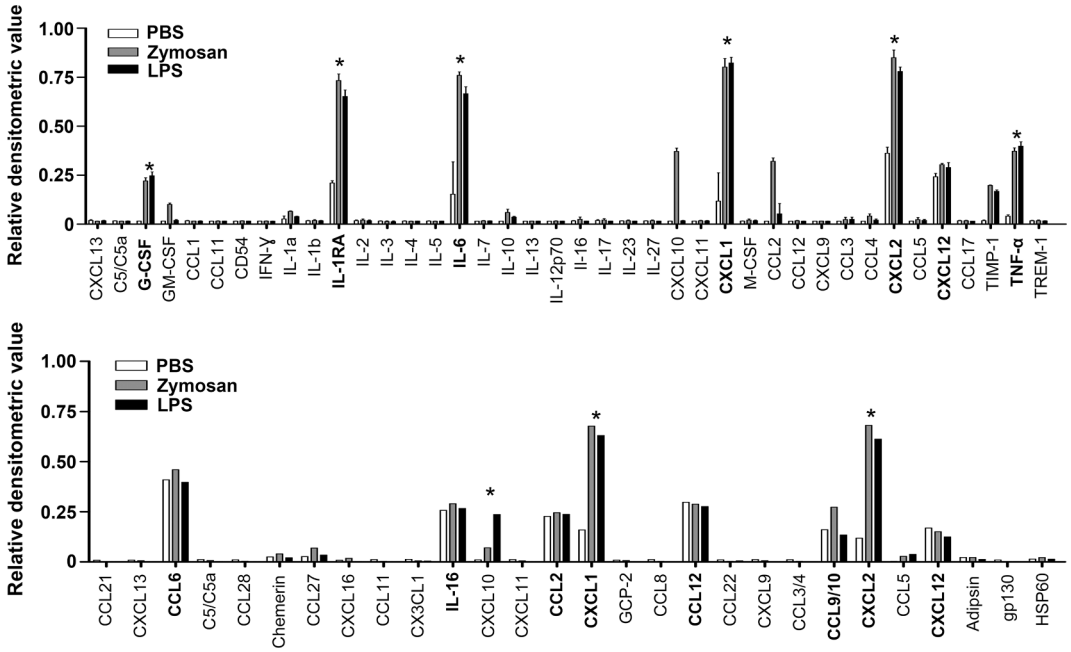

Fig. 3. *In vitro* TLR triggering induces the expression of pro-inflammatory cytokines and chemokines by NDS nodes. Single NDS node from the peritoneal cavity of 4-week-old C57BL/6 mice were placed in 1 ml of RPMI1640 medium containing 10% FBS and treated with 1 μg/ml LPS or 50 μg/ml zymosan for 6 h. Cytokines and chemokines in the supernatants were detected using a Mouse Chemokine and Cytokine Array Kit (R&D Systems). Densitometric values were calculated from duplicate blots (n = 4) and data are means ± SDs. Bold indicates the increased or decreased cytokines and chemokines by TLR stimulation.

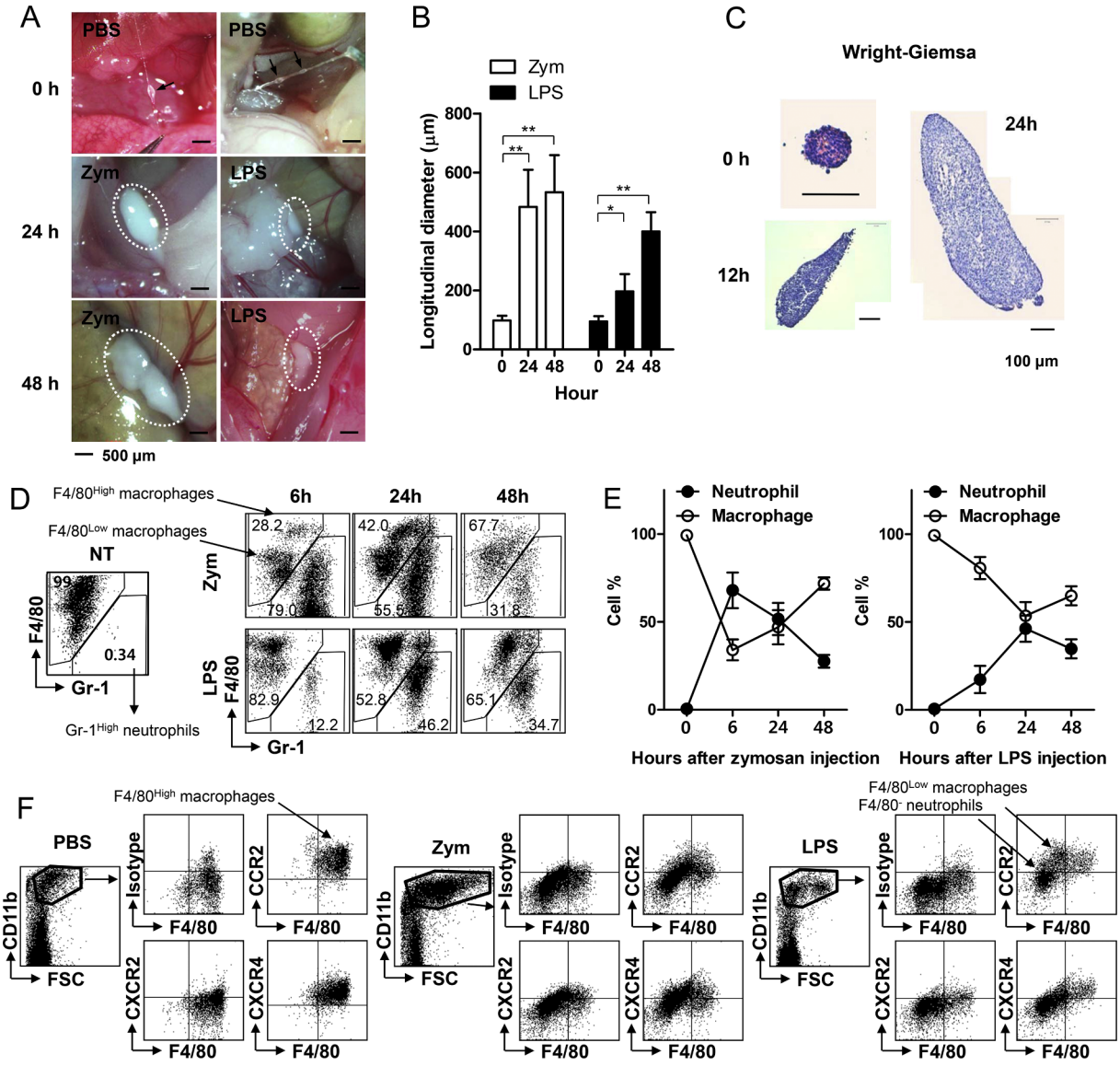

Fig. 4. Morphological and cellular changes of NDS node following TLR2/4 stimulation *in vivo*. Four-week-old male C57BL/6 mice were i.p. injected with 20 μg LPS or 200 μg zymosan. (A) NDSs from the peritoneal cavity were photographed under stereo microscope at the indicated time-points. (B) Median diameters of the collected NDS node were calculated from (A). (C) Frozen sections were prepared from the collected NDS nodes 0, 12 and 24 h after the injection of LPS, and stained with Wright-Giemsa solution. (D) NDS node cells were prepared 0, 6, 24, and 48 h after LPS or zymosan injection and stained with mAbs specific to CD11b, Gr-1, and F4/80. $CD11b^+$ cells were gated and plotted as F4/80 vs. Gr-1. $CD11b^+F4/80^{High}$ macrophages are indicated in blue dotted circle and $CD11b^+F4/80^{Low}$ macrophages are in red dotted circle. (E) Kinetics of percentages of $CD11b^+Gr\text{-}1^+$ neutrophils and $CD11b^+F4/80^+$ macrophages including $F4/80^{High}$ and $F4/80^{Low}$ cells in NDS node following TLR stimulation. (F) NDS cells were prepared 0 and 24 h after LPS or zymosan injection via i.p. route, stained with PE-conjugated anti-CCR2, anti-CXCR2, or anti-CXCR4 mAb as well as anti-CD11b and anti-F4/80 mAb. All samples were subsequently analyzed by FACSCalbur (BD Bioscience). Data are representative of at least three independent experiments (n = 2–4). Results in (B) and (E) are mean ± SD (*, $p < 0.05$; **, $p < 0.01$).

Measurements indicated that LPS or zymosan injection led to a 5–8-fold increase in the size of NDS nodes within 48 h (Fig. 4B). When frozen sections of the nodes were stained with Wright-Giemsa solution, it was evident that TLR4 triggering strongly increased the immune cells in the NDS nodes (Fig. 4C).

NDS node cells were analyzed by flow cytometry to identify resident immune subsets. Around 1–3% of the cells were $CD3^+$, $CD19^+$, $NK1.1^+$ cells as in naïve nodes even after injection of LPS or zymosan (data not shown). Again, $CD11b^+$ cells were the dominant population in LPS- or zymosan-primed nodes (data not shown). When $CD11b^+$ cells were plotted to $F4/80^+$ vs. $Gr\text{-}1^+$ to discriminate macrophages from neutrophils, $F4/80^{High}$ macrophages were the major population of NDS node in the steady state, while LPS or zymosan treatment rapidly decreased frequencies of $F4/80^{High}$ macrophages and increased frequencies of $Gr\text{-}1^{High}$ neutrophils and $F4/80^{Low}$ macrophages (Fig. 4D). Repeated experiments confirmed that neutrophil frequencies were transiently increased by both LPS and zymosan injection, whereas numbers of $F4/80^{Low}$ macrophages were only transiently increased by LPS treatment but continuously increased by zymosan treatment until 48 h after the injection (Fig. 4D). Moreover, it was notable that neutrophils peaked at 6 h in zymosan-primed NDS and at 24 h in LPS-primed NDS (Fig. 4E).

Neutrophils and $F4/80^{Low}$ macrophages were accumulated in NDS following LPS or zymosan injection (Fig. 4D) and several chemokines including CXCL1, CXCL2, CCL2, CCL6 and CXCL12 were secreted from NDS nodes (Fig. 3). Therefore, their receptors - CXCR2, CXCR4 and CCR2 were examined on macrophages and neutrophils in NDS nodes before and after LPS or zymosan injection. Most of $CD11b^+$ cells in NDS

nodes under steady status were F4/80^{High} macrophages with high level of CCR2 and CXCR4 and basal level of CXCR2 (Fig. 4F; left). Zymsan or LPS injection increased CD11b^{+}F4/80^{-} neutrophils and CD11b^{+}F4/80^{Low} macrophages in nodes (Fig. 4F; middle and right). Neutrophils expressed basal level of CXCR2, CXCR2 and CXCR4, while F4/80^{Low} macrophages expressed CCR2, CXCR2 and CXCR4 (Fig. 4F: middle and right).

Taken together, these observations show that proinflammatory stimulation *in vivo* with LPS or zymosan rapidly expands the volume of NDS nodes and increase numbers of Gr-1^{High} neutrophils and F4/80^{Low} macrophages. This suggests that NDS is immunological organs specialized in myeloid cell-related functions.

3.5. Apoptotic tumor cells increase neutrophils and macrophages in the hollow structure of NDS

Since we found dynamic morphological and cellular changes of NDS node in response to pathogen-associated molecular patterns (PAMPs) like LPS or zymosan, we next examined whether NDS responded to damage-associated molecular patterns (DAMPs). We injected apoptotic MC38 tumor cells into WT, TLR2$^{-/-}$, and TLR4$^{-/-}$ mice because many types of DAMP are recognized by TLR2 and TLR4 [28]. Injection of apoptotic tumor cells induced rapid swelling of NDS node in the WT mice (Fig. 5A; left panel). NDS nodes were barely found in TLR2$^{-/-}$ and TLR4$^{-/-}$ mice under steady state conditions, but could be detected and isolated following injection of the apoptotic tumor cells, although the swelling of NDS node was impaired in the TLR2$^{-/-}$ or TLR4$^{-/-}$ mice (Fig. 5A; middle and right panels). NDS node swelling was delayed and severely impaired in the absence of TLR2, but was more temporal in the absence of TLR4 signals (Fig. 5A). Again, lymphocytes and NK cells were rare under any conditions (data not shown), while F4/80^{Low} macrophages and Gr-1^{High} neutrophils accumulated massively in the NDS node of WT mice and peaked at 24–48 h (Fig. 5B; left panel). Numbers of CD11b^{+} cells, both macrophages and neutrophils, were much lower in the TLR2$^{-/-}$ mice than in the WT mice following injection of apoptotic tumor cells (Fig. 4B). Statistical analysis also indicated that the frequencies of CD11b^{+} cells were significantly lower in the TLR2$^{-/-}$ mice than in the WT mice and were more temporally peaked in the TLR4$^{-/-}$ mice than in the WT mice (Fig. 5C), and the recruitment and accumulation of neutrophils became temporal in the TLR2$^{-/-}$ or TLR4$^{-/-}$ mice than in the WT mice (Fig. 5C and D).

To determine the location of the macrophages and neutrophils in the swollen NDS nodes, frozen sections of WT NDS node were stained for CD11b, F4/80, or ER-TR7. F4/80^{High} cells were primarily localized in the marginal region of the node structure, while CD11b^{+} cells were widespread in the median region (Fig. 5E). Staining of ER-TR7 – a marker for reticular fibroblasts and reticular fibers – indicated that the swollen nodes had a hollow structure as their median region was negative for ER-TR7 (Fig. 5E and Supplemental Fig. 1). However, when freshly isolated NDS nodes were stained for ER-TR7, no hollow structures were evident, but numerous small chambers could be seen (Fig. 5F and Supplemental Movie 1). Since ER-TR-positive fibroblastic reticular cells (FRC) and the reticular network (RN) provide strong flexibility to swollen lymph nodes [29], the rapid accumulation of neutrophils and macrophages in naïve NDS node would appear to inflate the pre-existing FRC/RNs and hollow structures are created by accumulating the migrating cells to the inside of the NDS node.

3.6. CD11b^{+}F4/80^{Low} inflammatory macrophages migrate into the NDS node and induce the NDS node swelling

Although we found the swelling of NDS node and the accumulation of macrophages and neutrophils in NDS node, it was not clear whether the node was actively recruiting the inflammatory myeloid cells or the inflammatory myeloid cells were tended to be migrated and accumulated in nearby NDS nodes. To answer this question, we infused the leukocytes from GFP-transgenic B6 mice into WT B6 mice following the injection of zymosan or LPS, but hardly any GFP^{+} cells were observed among them (Supplemental Fig. 2). Next, peritoneal exudate cells (PECs) were isolated from LPS- or zymosan-injected B6 mice after 48 h, labeled with CFSE, and injected i.p. into B6 mice. One day after transfer, we found that the NDS nodes were moderately swollen in the injected mice (Fig. 6A and B). Moreover, 5–10% of the cells in the swollen nodes were CFSE^{+} cells, mainly CD11b^{+}F4/80^{Low} cells (Fig. 6C).

CD11b^{+}F4/80^{High} macrophages were the dominant cells in steady state HAR-Ns, whereas CD11b^{+}F4/80^{Low} macrophages and neutrophils became the prevalent populations for a time in stimulated NDS (Fig. 4D). Moreover, CD11b^{+}F4/80^{Low} macrophages spontaneously migrated into naïve NDS node and induced their swelling (Fig. 6C). Because CD11b^{+}F4/80^{Low} macrophages and neutrophils are the inflammatory innate immune cells secreting chemokines and cytokines, these results suggest that the macrophages and neutrophils migrated into the local inflammation site are intrinsically accumulated in the NDS node, amplifies the inflammatory cytokines and chemokines and thus, signals the presence of inflammation site to the immune system.

4. Discussion

In this study we demonstrate that NDS is primarily occupied by CD11b^{+}F4/80^{High} macrophages in the steady state and this population is rapidly and transiently replaced by CD11b^{+}F4/80^{Low} macrophages and CD11b^{+}F4/80^{-}Gr-1^{+} neutrophils following proinflammatory stimuli or apoptotic cells (Figs. 4D and 5A). This change is accompanied by rapid swelling of the NDS nodes (Figs. 4A and 5A). NDS nodes appear to swell rapidly by inflating the pre-existing FRC/RN (Fig. 5E) and harbor the accumulating macrophages and neutrophils in their inner region (Fig. 5C). Since TLR2 and TLR4 triggering led to preferential increase in cytokines and chemokines like CXCL1, CXCL2, CCL2, CCL6 and CXCL12 that are known to have chemotactic effects on macrophages and neutrophils (Fig. 3) [17,18,23,24,27], it was reasonable to expect that the rapid swelling of NDS might be initiated by increasing the inflammatory cytokines and chemokines from NDS. Moreover, the inward migration of CD11b^{+}F4/80^{Low} macrophages leads to expansion of naïve NDS node (Fig. 6). Considering that the NDS may form a spoke-hub pattern throughout the body [3], these results indicate that it functions as a hub to amplify local inflammation and to signal local infection systemically during the early phase of infections.

There have been reports of the existence of tertiary lymphoid tissues such as gut-associated lymphoid tissue (GALT), mucosa-associated lymphoid tissue (MALT), ectopic lymphoid structures (ELS), and fat-associated lymphoid clusters (FALC) [30–32]. Crucial differences between NDS and these lymphoid tissues or lymph nodes relate to the presence/absence of T and B lymphocytes. The major immune cells in lymph nodes, GALT, MALT, ELS, and FALC are lymphocytes [30–32], while the NDS contains innate immune cells as the major population - macrophages in the steady state, and macrophages/neutrophils in the inflamed state (Fig. 4D and E). Since the predominance of myeloid cells is the key feature of NDS, we speculate that the NDS is an immune organ specialized in myeloid cells.

When we analyzed NDS node cells by flow cytometry, the majority were of CD11b^{+}F4/80^{High} phenotype (Fig. 2A). Moreover, proinflammatory stimuli massively increased CD11b^{+}F4/80^{Low} macrophages and neutrophils in these nodes (Fig. 4D). A similar phenotype was found for the macrophages in the peritoneal cavity of mice (Fig. 2D) [33]: CD11b^{+}F4/80^{High} large peritoneal macrophages (LPM) were the main population in the steady state, and CD11b^{+}F4/80^{Low} small peritoneal macrophages (SPM) were the predominant population in the inflamed peritoneum [34]. Murine blood monocytes are very different from SPMs and LPMs as they have CD11b^{Low}F4/80^{Low} phenotypes (Fig. 2D) [34]. LPMs appear to be maintained by self-renewal in the steady state and are known to originate from the yolk sac [34],

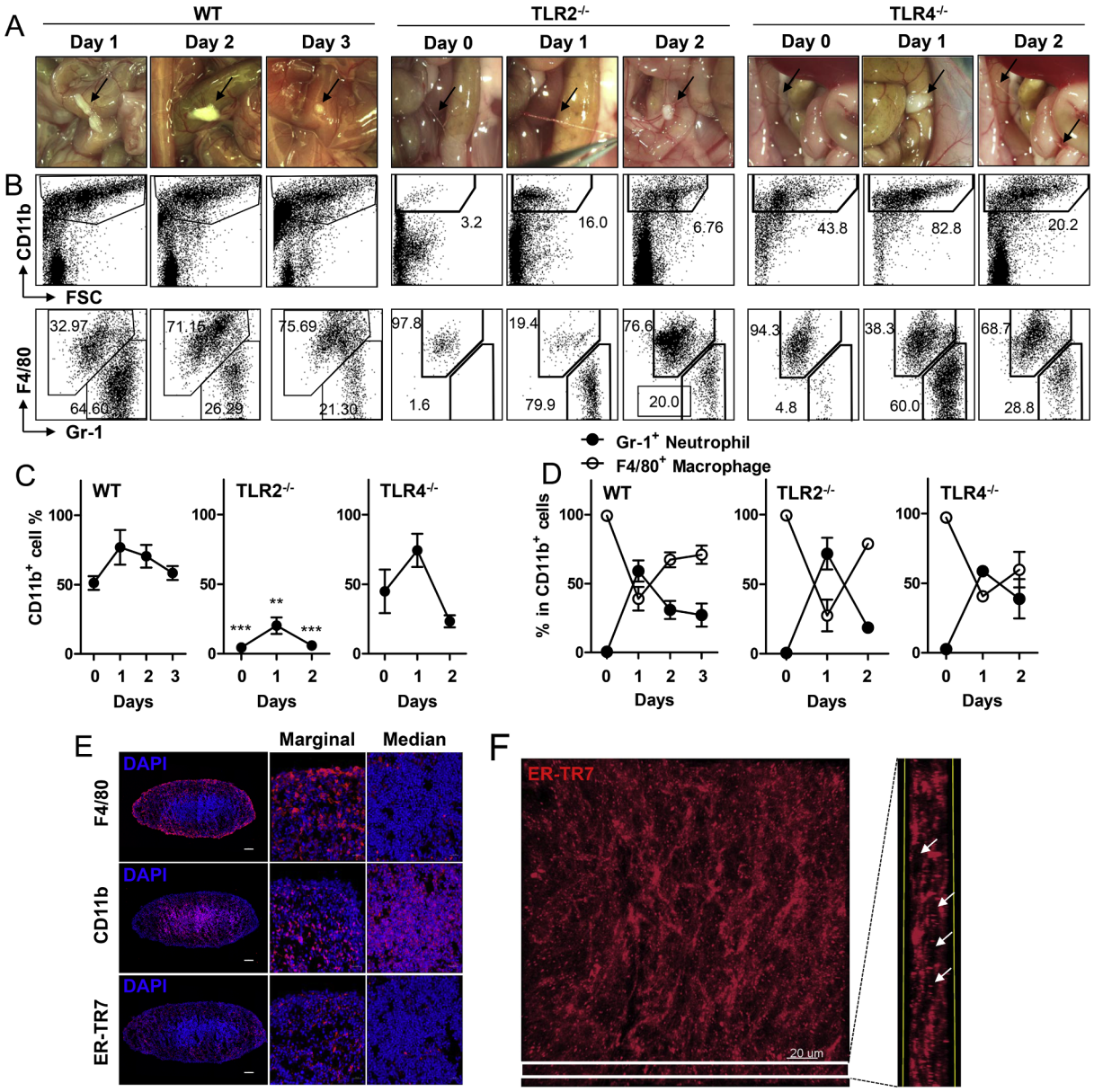

Fig. 5. Impaired NDS node swelling in the absence of TLR2 or TLR4 signals, and the hollow structure of swollen NDS node. C57BL/6, TLR2$^{-/-}$, and TLR4$^{-/-}$ mice were i.p. injected with 1×10^7 irradiated apoptotic MC37 tumor cells. (A) NDS were photographed under a stereo microscope at the indicated days. (B) NDS node cells were stained with mAbs specific to CD11b, F4/80, and Gr-1, and subsequently analyzed by FACSCalibur (BD Bioscience). CD11b$^+$ cells were gated and plotted as F4/80 vs. Gr-1. (C and D) Percentages of total CD11b$^+$ cells, and F4/80$^+$ or Gr-1$^+$ cells among CD11b$^+$ cells were calculated from (B). *P*-values of (B) were calculated by comparing CD11b$^+$ cell % of TLR2$^{-/-}$ NDS with that of WT NDS. (E) NDS nodes from WT mice were collected 24 h after injection of irradiated MC38 tumor cells. Ten-μm-thick frozen sections were stained with anti-F4/80, CD11b, and ER-TR7 antibodies, and the slides were mounted with DAPI-containing solution. Images were captured by laser scanning microscope (Zeiss LSM 780, Carl Zeiss, Germany). Scale bar = 100 μm. (F) Whole mount and sectional view of NDS nodes. The fixed NDS node was stained for anti-ER-TR7 mAb. Z-stack images were acquired with a laser scanning microscope (Zeiss LSM 780) and projected as a maximum intensity projection. Data are representative of three independent experiments (n = 3). Results in (C) and (D) are mean ± SD.

while SPMs are generated by differentiation of circulating blood monocytes and short-lived cells [35,36]. The CD11b$^+$F4/80^{High} and CD11b$^+$F4/80^{Low} macrophages found in NDS nodes seem to be identical to LPMs and SPMs because naïve NDS nodes mainly contain CD11b$^+$F4/80^{High} macrophages, and proinflammatory stimuli massively increases CD11b$^+$F4/80^{Low} macrophages (Fig. 4D and E). Therefore, we suspect that the CD11b$^+$F4/80^{High} macrophages in NDS nodes may have similar properties to tissue macrophages.

Tissue macrophages originate from the yolk sac during embryonic development, and the fetal liver and bone marrow development follows later [35]. Although resident tissue macrophages originate from the same yolk sac, their functions and roles are highly organ-specific [35]. In this study, we collected the NDS node cells from the peritoneal cavity and found that their phenotypes were identical with that of peritoneal macrophages. However, considering that NDS nodes exist throughout the body, it is possible that the phenotypes and functions of macrophages in HAR nodes differ in different organs.

It has been reported that the NDS in the vitelline membrane of eggs develop earlier than those in the extraembryonic vessels, heart, and intramembrane vessels [36]. The tissue macrophages are also generated from the yolk sac before development of the fetal liver and bone marrow, and play crucial roles in regulating embryonic vascular growth and patterning [37]. Since the tissue macrophages derived from the yolk sac are crucial for the development of organs and vasculature

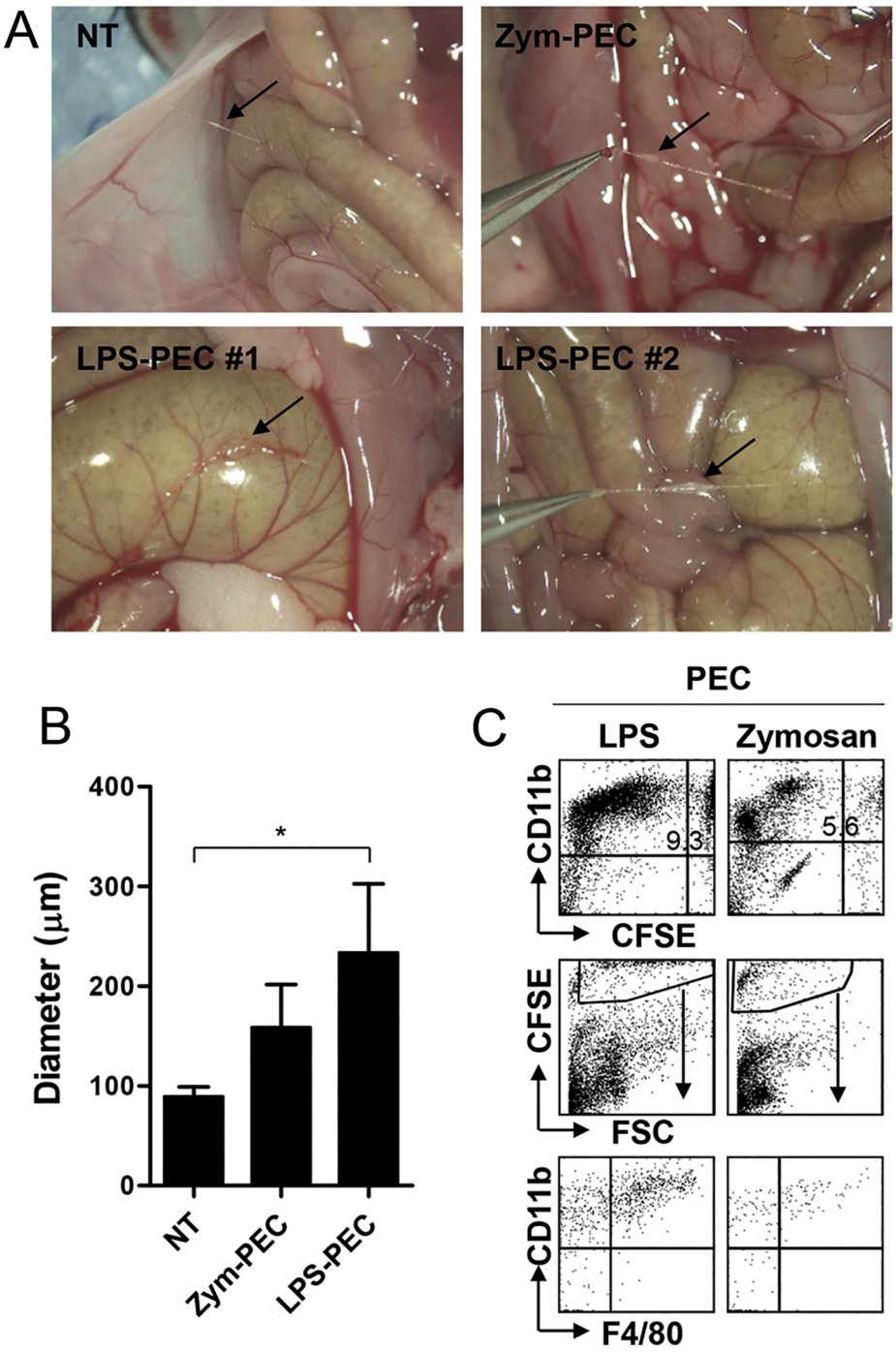

Fig. 6. Inward migration of $CD11b^{+}F4/80^{Low}$ macrophages into NDS nodes *in vivo*. Peritoneal exudate cells (PECs) were collected from C57BL/6 mice 2 days after the injection of 20 μg LPS or 200 μg zymosan, labeled with 10 μM CFSE, and then i.p injected into C57BL/6 mice. After 24 hr, NDS nodes were photographed under a stereo microscope (A) and the size of NDS nodes was calculated (B). NDS node cells were stained with anti-CD11b and anti-F4/80 mAbs, and the percentages and phenotypes of $CFSE^{+}$ cells were determined by flow cytometry. Data are representative of three independent experiments (n = 3). Results in (B) are means ± SDs (*, $p < 0.05$).

[37–39], it is possible that NDS first develop during embryogenesis along with the development of tissue macrophages and then participate in organ development and provide protection from pathogens until the immune system has fully developed. Similar with the lymphoid tissues, the NDS has a flexible structure, is structured with the fibroblastic reticular cells and reticular network, and networked in the body through nodes and ducts [3]. One difference between NDS and lymphoid system was the cell types – myeloid vs. lymphoid cells. Therefore, our data also provide a possibility that NDS may be the primordial type of immune system in lower organisms and provide a blueprint for the evolution of the lymphoid system in higher organisms.

Taken together, our findings suggest that NDS is an immune organ specialized in myeloid cells and function as a hub to amplify local inflammation and to signal local infection systemically during the early phase of infections (Supplemental Fig. 3).

Acknowledgement

This work was funded by grants from the National Cancer Center of Korea (NCC-1610320 & NCC-1810102), the Korean Ministry of Trade, Industry and Energy (GLOBAL R&D PROJECT, N0000901), and Ministry of Health and Welfare Grant (KDDF 201408-2).

Competing interests

S.H.H. and B.S.K. are employed by Eutilex and B.S.K. has equity ownership in Eutilex. B.K.C., Y.I.K., and R.S. declare no conflicts of interest.

Appendix A. Supplementary material

Supplementary data associated with this article can be found, in the online version, at https://doi.org/10.1016/j.cyto.2018.06.011.

References

[1] B.H. Kim, Research on the Kyungrak, J. Acad. Med. Sci. DPR Kor. 9 (1962) 5–13.
[2] B.H. Kim, On the Kyungrak system, J. Acad. Med. Sci. DPR Kor. 108 (1965) 1–38.
[3] K.S. Soh, K.A. Kang, Y.H. Ryu, 50 years of bong-han theory and 10 years of primo vascular system, Evid. Based Complem. Alternat. Med. 2013 (2013) 587827.
[4] K.S. Soh, Bonghan circulatory system as an extension of acupuncture meridians, J. Acupunct. Meridian Stud. 2 (2009) 93–106.
[5] B.C. Lee, K.Y. Baik, H.M. Johng, et al., Acridine orange staining method to reveal the characteristic features of an intravascular threadlike structure, Anat. Rec. B New Anat. 278 (2004) 27–30.
[6] B.C. Lee, J.S. Yoo, K.Y. Baik, et al., Novel threadlike structures (Bonghan ducts) inside lymphatic vessels of rabbits visualized with a Janus Green B staining method, Anat. Rec. B New Anat. 286 (2005) 1–7.
[7] C. Lee, S.K. Seol, B.C. Lee, et al., Alcian blue staining method to visualize bonghan threads inside large caliber lymphatic vessels and x-ray microtomography to reveal their microchannels, Lymphat. Res. Biol. 4 (2006) 181–190.
[8] B.C. Lee, K.W. Kim, K.S. Soh, Visualizing the network of Bonghan ducts in the omentum and peritoneum by using Trypan blue, J. Acupunct. Meridian Stud. 2 (2009) 66–70.
[9] J.S. Yoo, H.B. Kim, V. Ogay, et al., Bonghan ducts as possible pathways for cancer metastasis, J. Acupunct. Meridian Stud. 2 (2009) 118–123.
[10] E.S. Park, J.H. Lee, W.J. Kim, et al., Expression of stem cell markers in primo vessel of rat, Evid. Based Complem. Alternat. Med. 2013 (2013) 438079.
[11] A. Ping, S. Zhendong, D. Jingxing, et al., Discovery of endothelium and mesenchymal properties of primo vessels in the mesentery, Evid. Based Complem. Alternat. Med. 2013 (2013) 205951.
[12] B.C. Lee, B. Sung, K.H. Eom, et al., Novel threadlike structures on the surfaces of mammalian abdominal organs are loose bundles of fibrous stroma with microchannels embedded with fibroblasts and inflammatory cells, Conn. Tiss. Res. 54 (2013) 94–100.
[13] B.S. Kwon, C.M. Ha, S. Yu, et al., Microscopic nodes and ducts inside lymphatics and on the surface of internal organs are rich in granulocytes and secretory granules, Cytokine 60 (2012) 587–592.
[14] S. Hwang, S.J. Lee, S.H. Park, et al., Nonmarrow hematopoiesis occurs in a hyaluronic-acid-rich node and duct system in mice, Stem Cells Dev. 23 (2014) 2661–2671.
[15] A. Cassado Ados, M.R. D'Império Lima, K.R. Bortoluci, Revisiting mouse peritoneal macrophages: heterogeneity, development, and function, Front. Immunol. 6 (2015) 225.
[16] A.W. Roberts, G-CSF: a key regulator of neutrophil production, but that's not all!, Growth Fact. 23 (2005) 33–41.
[17] S.D. Wolpe, B. Sherry, D. Juers, et al., Identification and characterization of macrophage inflammatory protein 2, Proc. Natl. Acad. Sci. USA 86 (1989) 612–616.
[18] C. Schumacher, I. Clark-Lewis, M. Baggiolini, B. Moser, High- and low-affinity binding of GRO alpha and neutrophil-activating peptide 2 to interleukin 8 receptors on human neutrophils, Proc. Natl. Acad. Sci. USA 89 (1992) 10542–10546.
[19] S.M. Hurst, T.S. Wilkinson, R.M. McLoughlin, et al., IL-6 and its soluble receptor orchestrate a temporal switch in the pattern of leukocyte recruitment seen during acute inflammation, Immunity 14 (2001) 705–714.
[20] E. Esposito, S. Cuzzocrea, TNF-alpha as a therapeutic target in inflammatory diseases, ischemia-reperfusion injury and trauma, Curr. Med. Chem. 16 (2009) 3152–3167.
[21] R. Horai, S. Saijo, H. Tanioka, et al., Development of chronic inflammatory arthropathy resembling rheumatoid arthritis in interleukin 1 receptor antagonist-deficient mice, J. Exp. Med. 191 (2000) 313–320.
[22] V.C. Asensio, S. Lassmann, A. Pagenstecher, et al., C10 is a novel chemokine expressed in experimental inflammatory demyelinating disorders that promotes recruitment of macrophages to the central nervous system, Am. J. Pathol. 154 (1999) 1181–1191.
[23] M.S. Berger, D.D. Taub, A. Orlofsky, et al., The chemokine C10: immunological and functional analysis of the sequence encoded by the novel second exon, Cytokine 8 (1996) 439–447.
[24] M. Chatterjee, S.N. von Ungern-Sternberg, P. Seizer, et al., Platelet-derived CXCL12 regulates monocyte function, survival, differentiation into macrophages and foam cells through differential involvement of CXCR4-CXCR7, Cell Death Dis. 6 (2015) e1989.
[25] X. Zhao, A. Sato, S.C. Dela Cruz, et al., CCL9 is secreted by the follicle-associated epithelium and recruits dome region Peyer's patch CD11b+ dendritic cells, J. Immunol. 171 (2003) 2797–2803.
[26] W.W. Cruikshank, H. Kornfeld, D.M. Center, Interleukin-16, J. Leukoc. Biol. 67 (2000) 757–766.
[27] S.L. Deshmane, S. Kremlev, S. Amini, et al., Monocyte chemoattractant protein-1 (MCP-1): an overview, J. Interf. Cytok. Res. 29 (2009) 313–326.
[28] A.M. Piccinini, K.S. Midwood, DAMPening inflammation by modulating TLR signalling, Mediat. Inflamm. 2010 (2010) 672395.
[29] A. Link, T.K. Vogt, S. Favre, et al., Fibroblastic reticular cells in lymph nodes regulate the homeostasis of naive T cells, Nat. Immunol. 8 (2007) 1255–1265.
[30] R. Pabst, Plasticity and heterogeneity of lymphoid organs. What are the criteria to call a lymphoid organ primary, secondary or tertiary? Immunol. Lett. 15 (112) (2007) 1–8.
[31] S. Finkin, D. Yuan, I. Stein, et al., Ectopic lymphoid structures function as microniches for tumor progenitor cells in hepatocellular carcinoma, Nat. Immunol. 16 (2015) 1235–1244.
[32] K. Moro, T. Yamada, M. Tanabe, et al., Innate production of T(H)2 cytokines by adipose tissue-associated c-Kit(+)Sca-1(+) lymphoid cells, Nature 463 (2010) 540–544.
[33] E.E. Ghosn, A.A. Cassado, G.R. Govoni, et al., Two physically, functionally, and developmentally distinct peritoneal macrophage subsets, Proc. Natl. Acad. Sci. USA 107 (2010) 2568–2573.
[34] D.W. Cain, E.G. O'Koren, M.J. Kan, et al., Identification of a tissue-specific, C/EBPβ-dependent pathway of differentiation for murine peritoneal macrophages, J. Immunol. 191 (2013) 4665–4675.
[35] S. Epelman, K.J. Lavine, G.J. Randolph, Origin and functions of tissue macrophages, Immunity 41 (2014) 21–35.
[36] K.S. Soh, K.A. Kang, D. Harrison, Development of the putative primo vascular system before the formation of vitelline vessels in chick embryos, The Primo Vascular System, its Role in Cancer and Regeneration, Springer, NY, 2001, pp. 77–82.
[37] X.M. Dai, G.R. Ryan, A.J. Hapel, et al., Targeted disruption of the mouse colony-stimulating factor 1 receptor gene results in osteopetrosis, mononuclear phagocyte deficiency, increased primitive progenitor cell frequencies, and reproductive defects, Blood 99 (2002) 111–120.
[38] S.R. McKercher, B.E. Torbett, K.L. Anderson, et al., Targeted disruption of the PU.1 gene results in multiple hematopoietic abnormalities, EMBO J. 15 (1996) 5647–5658.
[39] W. Wiktor-Jedrzejczak, A. Bartocci Jr., A.W. Ferrante, et al., Total absence of colony-stimulating factor 1 in the macrophage-deficient osteopetrotic (op/op) mouse, Proc. Natl. Acad. Sci. USA 87 (1990) 4828–4832.